Circulation Research

ORIGINAL RESEARCH

SIRT3 Regulates Clearance of Apoptotic Cardiomyocytes by Deacetylating Frataxin

Jing Gao, Chenglin Huang, Linghui Kong, Wugang Zhou, Mengwei Sun, Tong Wei, Weili Shen

BACKGROUND: Efferocytosis is an activity of macrophages that is pivotal for the resolution of inflammation in hypertension. The precise mechanism by which macrophages coordinate efferocytosis and internalize apoptotic cardiomyocytes remains unknown. The aim of this study was to determine whether SIRT3 (sirtuin-3) is required for both apoptotic cardiomyocyte engulfment and anti-inflammatory responses during efferocytosis.

METHODS: We generated myeloid SIRT3 knockout mice and FXN (frataxin) knock-in mice carrying an acetylation-defective lysine to arginine K189R mutation (FXN^{K189R}). The mice were given Ang II (angiotensin II) infusion for 7 days. We analyzed cardiac macrophages' mitochondrial iron levels, efferocytosis activity, and phenotype both in vivo and in vitro.

RESULTS: We showed that SIRT3 deficiency exacerbated Ang II–induced downregulation of the efferocytosis receptor MerTK (c-Mer tyrosine kinase) and proinflammatory cytokine production, accompanied by disrupted mitochondrial iron homeostasis in cardiac macrophages. Quantitative acetylome analysis revealed that SIRT3 deacetylated FXN at lysine 189. Ang II attenuated SIRT3 activity and enhanced the acetylation level of FXN^{K189}. Acetylated FXN further reduced the synthesis of ISCs (iron-sulfur clusters), resulting in mitochondrial iron accumulation. Phagocytic internalization of apoptotic cardiomyocytes increased myoglobin content, and derived iron ions promoted mitochondrial iron overload and lipid peroxidation. An iron chelator deferoxamine improved the levels of MerTK and efferocytosis, thereby attenuating proinflammatory macrophage activation. FXN^{K189R} mice showed improved macrophage efferocytosis, reduced cardiac inflammation, and suppressed cardiac fibrosis.

CONCLUSIONS: The SIRT3-FXN axis has the potential to resolve cardiac inflammation by increasing macrophage efferocytosis and anti-inflammatory activities.

GRAPHIC ABSTRACT: A graphic abstract is available for this article.

Key Words: c-Mer tyrosine kinase ■ ions ■ macrophages ■ phenotype ■ sirtuin 3

Meet the First Author, see p 541 | Editorial, see p 648

Cardiomyocyte apoptosis is abundant in hypertrophic hearts of patients with hypertension. It is induced by various factors such as pressure overload and angiotensin.[1] Mobilization of macrophages to clear and metabolize apoptotic cardiomyocytes (ACs) is essential for repair after cardiac injury. Efficient clearance of ACs by macrophages, also known as efferocytosis, prevents postapoptotic necrosis and reduces inflammation, whereas defective efferocytosis contributes to persistent myocardial inflammation and dysfunction.[2,3] Therefore, enhancing efferocytosis has been proposed as a therapeutic strategy for the treatment of hypertensive heart disease.

Recent studies have suggested that the efferocytosis capacity of macrophages relies on mitochondrial function.[4] As the ingestion of ACs by macrophages leads to

Correspondence to: Weili Shen, PhD, Department of Cardiovascular Medicine, State Key Laboratory of Medical Genomics, Shanghai Key Laboratory of Hypertension, Shanghai Institute of Hypertension, Ruijin Hospital, Shanghai Jiao Tong University School of Medicine, Shanghai, China. Email wlshen@sibs.ac.cn
Supplemental Material is available at https://www.ahajournals.org/doi/suppl/10.1161/CIRCRESAHA.123.323160.
For Sources of Funding and Disclosures, see page 646.

Circulation Research is available at www.ahajournals.org/journal/res

ORIGINAL RESEARCH

Novelty and Significance

What Is Known?

- Efficient clearance of apoptotic cardiomyocytes (ACs) through efferocytosis is essential for resolving cardiac inflammation.
- Disruption of mitochondrial metabolic function has been shown to contribute to defective efferocytosis.
- SIRT3 (sirtuin-3) plays a crucial role in regulating mitochondrial function by modifying proteins through deacetylation.

What New Information Does This Article Contribute?

- Mitochondrial iron disorders result in defective clearance of ACs.
- SIRT3 regulates mitochondrial iron metabolism by deacetylating FXN (frataxin) at lysine 189.
- Engulfment of ACs elevates mitochondrial iron uptake.
- The SIRT3-FXN axis links iron metabolism efflux and apoptotic cell clearance.

Efferocytosis—the process of clearing ACs—is crucial for resolving cardiac inflammation. The metabolic substrates from apoptotic cells, known as efferocytosis catabolism, can directly affect macrophage function. We found that Ang II (angiotensin II) impairs SIRT3 activity, leading to elevated acetylation levels of FXN^{K189}. Acetylated FXN reduces the synthesis of iron-sulfur clusters, thereby causing mitochondrial iron accumulation. Phagocytosis of ACs increases myoglobin content, and the produced Fe^{2+} worsens Ang II–induced mitochondrial iron disorders. Heme-derived metabolites exacerbate mitochondrial labile iron and lipid peroxidation, leading to defective efferocytosis and proinflammatory macrophage activation via the NF-κB (nuclear factor kappa B) signaling pathway. We made the novel observation that the ability of myocardium-infiltrating macrophages to process iron determines myocardial degeneration.

Nonstandard Abbreviations and Acronyms

AC	apoptotic cardiomyocyte
Ang II	angiotensin II
BMDM	bone marrow–derived macrophage
CCR2	C-C motif chemokine receptor 2
FXN	frataxin
HO-1	hemeoxygenase-1
IL	interleukin
ISC	iron-sulfur cluster
MerTK	c-Mer tyrosine kinase
MHC-II	major histocompatibility complex II
NF-κB	nuclear factor kappa B
SIRT3	sirtuin-3
SIRT3 MKO	myeloid sirtuin-3 knockout
WT	wild type

the accumulation of metabolic cargo, including lipids, proteins, and nucleotides, the metabolic components have to be quickly degraded or redistributed within macrophages to maintain cellular homeostasis. According to the current literature, mice lacking myeloid Drp1 (dynamin-related protein 1) lose the ability to successively engulf apoptotic cells, which results in advanced atherosclerosis.[5] UCP2 (uncoupling protein 2) is an inner mitochondrial membrane protein, and it is upregulated in phagocytes that engulf apoptotic cells. Deficiency of UCP2 reduces apoptotic cell clearance and promotes atherosclerosis.[6] These data suggest that mitochondrial dysfunction in macrophages is closely associated with defective efferocytosis.

Myoglobin is a monomeric heme protein. It is mainly found in cardiomyocytes, where it serves as an intracellular storage for oxygen.[7] After engulfing ACs, macrophages process them to degrade myoglobin-associated heme, which is dissociated by HO-1 (hemeoxygenase-1) into Fe^{2+}, biliverdin, and carbon monoxide.[8] This implies that engulfment of ACs elevates macrophage iron uptake, whereas AC-derived iron may act as a major substrate for macrophage metabolism. Thus, it is considered that the ability of macrophages to process mitochondrial iron determines their mitochondrial function.

The mitochondria are recognized as the main hub of iron metabolism. FXN (frataxin) is a conserved mitochondrial protein encoded by the *frataxin* gene, which functions in the process of ISC (iron-sulfur cluster) synthesis and facilitates the assembly of mitochondrial ISC protein complexes such as aconitase, lipoate synthase, and succinate dehydrogenases.[9–11] FXN deficiency is responsible for the devastating rare hemochromatosis of Friedreich ataxia.[12] FXN insufficiency results in mitochondrial iron accumulation, extensive oxidative damage, loss of myelinated fibers, and subsequent cell death.[13–15] Previous studies have shown that FXN involves transcriptional[14,16] and posttranslational modification of regulatory networks. Highly acetylated FXN negatively correlates with the expression level of deacetylase SIRT3 (sirtuin-3).[17] Our previous study confirmed that Ang II (angiotensin II)—a hypertensive peptide—suppressed SIRT3 expression in mitochondria.[18–20] Several groups have reported the exacerbation

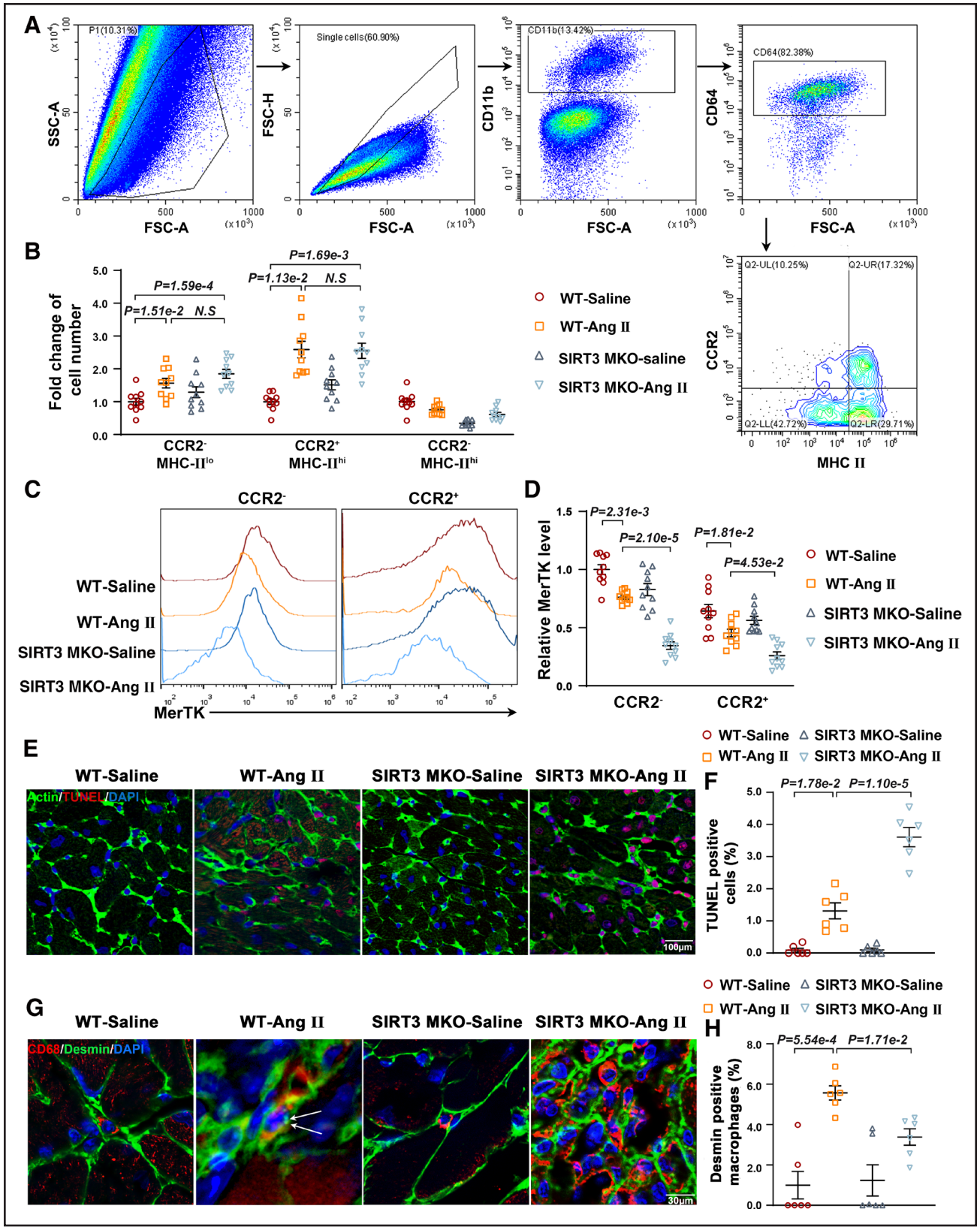

Figure 1. Defective efferocytosis and proinflammatory macrophage activation lead to myocardial inflammation.
A, Gating strategy for cardiac macrophages. Eight-week-old C57BL/6J (wild type [WT]) and SIRT3 (sirtuin-3) knockout (SIRT3 MKO) mice were given 1500 ng·kg^{-1}·min^{-1} of Ang II (angiotensin II) or saline for 7 days. **B**, Quantification of CD11b^{+}CD64^{+}CCR2 (C-C motif chemokine receptor 2)$^{-}$MHC-II (major histocompatibility complex II)^{lo}, CD11b^{+}CD64^{+}CCR2^{+}MHC-II^{hi}, and CD11b^{+}CD64^{+}CCR2^{-}MHC-II^{hi} cells (n=10 mice per group). Normal distribution was confirmed by the Shapiro-Wilk test. Significance of differences was examined by 2-way ANOVA followed (*Continued*)

of Ang II–induced iron overload and oxidative stress in SIRT3 deficiency.[21] Thus, SIRT3 may coordinate FXN to maintain mitochondrial iron homeostasis. However, the interaction between AC-derived iron and efferocytosis is still unclear.

Here, we hypothesized that Ang II inhibits SIRT3 expression and promotes FXN hyperacetylation modification, thereby leading to mitochondrial iron overload. Additionally, phagocytic internalization of ACs increases myoglobin content, and thus, derived Fe^{2+} deteriorates mitochondrial iron disorders. Mitochondrial iron overload further reduces efferocytosis and leads to secondary cardiac damage.

METHODS

Data Availability

A detailed description of the materials and methods can be found in the Supplementary Material. The data supporting the findings of this study are available from the corresponding author upon reasonable request.

RESULTS

Defective Efferocytosis and Activation of Proinflammatory Macrophages Leads to Myocardial Inflammation

Defective efferocytosis is a major cause of chronic myocardial inflammation that induces progressive structural damage and leads to cardiac fibrosis. Eight-week-old C57BL/6J (wild type [WT]) and SIRT3 knockout mice received 1500 $ng{\cdot}kg^{-1}{\cdot}min^{-1}$ of Ang II or saline for 7 days. We assessed cardiac macrophage populations adapting gating strategies to distinguish resident and recruited cells. Cardiac macrophages were identified as $CD11b^+$/$CD64^+$ (cluster of differentiation) cells, and they were subdivided into 3 distinct subsets based on the expression of MHC-II (major histocompatibility complex II) and CCR2 (C-C motif chemokine receptor 2), namely, $CCR2^-MHC\text{-}II^{lo}$, $CCR2^-MHC\text{-}II^{hi}$, and $CCR2^+MHC\text{-}II^{hi}$ macrophages. Ang II infusion increased the abundance of both $CCR2^+MHC\text{-}II^{hi}$ and $CCR2^-MHC\text{-}II^{lo}$ macrophages, whereas $CCR2^-MHC\text{-}II^{hi}$ macrophages remained comparable to the saline controls. SIRT3 deletion did not alter the macrophage populations induced by Ang II (Figure 1A and 1B). Compared with $CCR2^+$ macrophages, $CCR2^-$ macrophages under steady-state conditions exhibited higher levels of MerTK (c-Mer tyrosine kinase), an integral membrane protein that promotes efferocytosis and inhibits inflammatory signaling. However, treatment with Ang II reduced the surface expression of MerTK, and SIRT3 deletion exacerbated the reduction of MerTK in both $CCR2^-$ and $CCR2^+$ macrophages (Figure 1C and 1D).

Next, we generated conditional SIRT3 knockout mice based on LysM-Cre mice ($SIRT3^{fl/fl}$:LysM-$Cre^{+/+}$, myeloid SIRT3 knockout [SIRT3 MKO]; Figure S1A). Both $SIRT3^{fl/fl}$:LysM-$Cre^{-/-}$ (WT) and SIRT3 MKO mice were exposed to Ang II for 7 days. We found a similar increase in blood pressure during Ang II infusion in the WT and SIRT3 MKO groups (Figure S1B). However, collagen deposition and collagen I expression were greater in the SIRT3 MKO group than in the WT group (Figure S1C and S1D). We confirmed Ang II–induced ACs in vivo by TUNEL (terminal deoxynucleotidyl transferase dUTP nick-end labeling) staining. Myeloid SIRT3 deficiency led to a progressive accumulation of uncleared TUNEL-positive ACs compared with the control mice (Figure 1E and 1F). Next, we costained the myocardial sections for cardiomyocytes (desmin) and macrophages (CD68) to determine whether the obtained results were associated with defective efferocytosis. As hypothesized, administration of Ang II resulted in partial colocalization of yellow cardiomyocyte desmin signal with $CD68^+$ macrophages, and desmin-associated $CD68^+$ cells were further reduced in the SIRT3 MKO group (Figure 1G and 1H).

$CD11b^+$ cells were purified from the myocardium (Figure S1E) and analyzed by Western blotting for the expression of SIRT3 and phagocytosis receptor MerTK. Not only did Ang II inhibit SIRT3 expression, but it also decreased MerTK protein levels, which was further exacerbated in the SIRT3 MKO mice (Figure S1F). These data indicated that SIRT3 deficiency reduced efferocytosis of ACs under hypertensive conditions. This was accompanied with a proinflammatory and profibrotic milieu, with upregulation of the proinflammatory cytokines such as TNF-α (tumor necrosis factor alpha), iNOS (inducible NO

Figure 1 Continued. by Tukey multiple comparison tests. **C**, Representative flow cytometry images of MerTK (c-Mer tyrosine kinase) in $CD11b^+CD64^+CCR2^-$ or $CD11b^+CD64^+CCR2^+$ cells in the heart. **D**, Fluorescence intensity of MerTK in $CD11b^+CD64^+CCR2^-$ or $CD11b^+CD64^+CCR2^+$ cells in the heart (n=10 mice per group). Normal distribution was confirmed by the Shapiro-Wilk test. Significance of differences was examined by 2-way ANOVA followed by Tukey multiple comparison tests. **E**, Eight-week-old $SIRT3^{fl/fl}$:LysM-$Cre^{-/-}$(WT) and $SIRT3^{fl/fl}$:LysM-$Cre^{+/+}$ (myeloid SIRT3 KO [SIRT3 MKO]) mice were given 1500 $ng{\cdot}kg^{-1}{\cdot}min^{-1}$ of Ang II or saline for 7 days. Representative fluorescence micrographs of the sections of the heart labeled with TUNEL (terminal deoxynucleotidyl transferase dUTP nick-end labeling; red), α-actinin (green), and DAPI (4′,6-diamidino-2-phenylindole; blue). Scale bar, 100 μm. **F**, Number of TUNEL-positive nuclei presented as the percentage of the total number of nuclei in the sections of the heart (n=6 mice per group). Statistical analysis was performed by Kruskal-Wallis test followed by Dunn multiple comparisons tests. **G**, Representative fluorescence micrographs of the sections of the heart labeled with CD68 (red), desmin (green), and DAPI (blue). Scale bar, 30 μm. **H**, Number of desmin-positive nuclei presented as the percentage of the total number of nuclei in the sections of the heart (n=6 mice per group). Statistical analysis was performed by Kruskal-Wallis test followed by Dunn multiple comparisons tests. CD indicates cluster of differentiation.

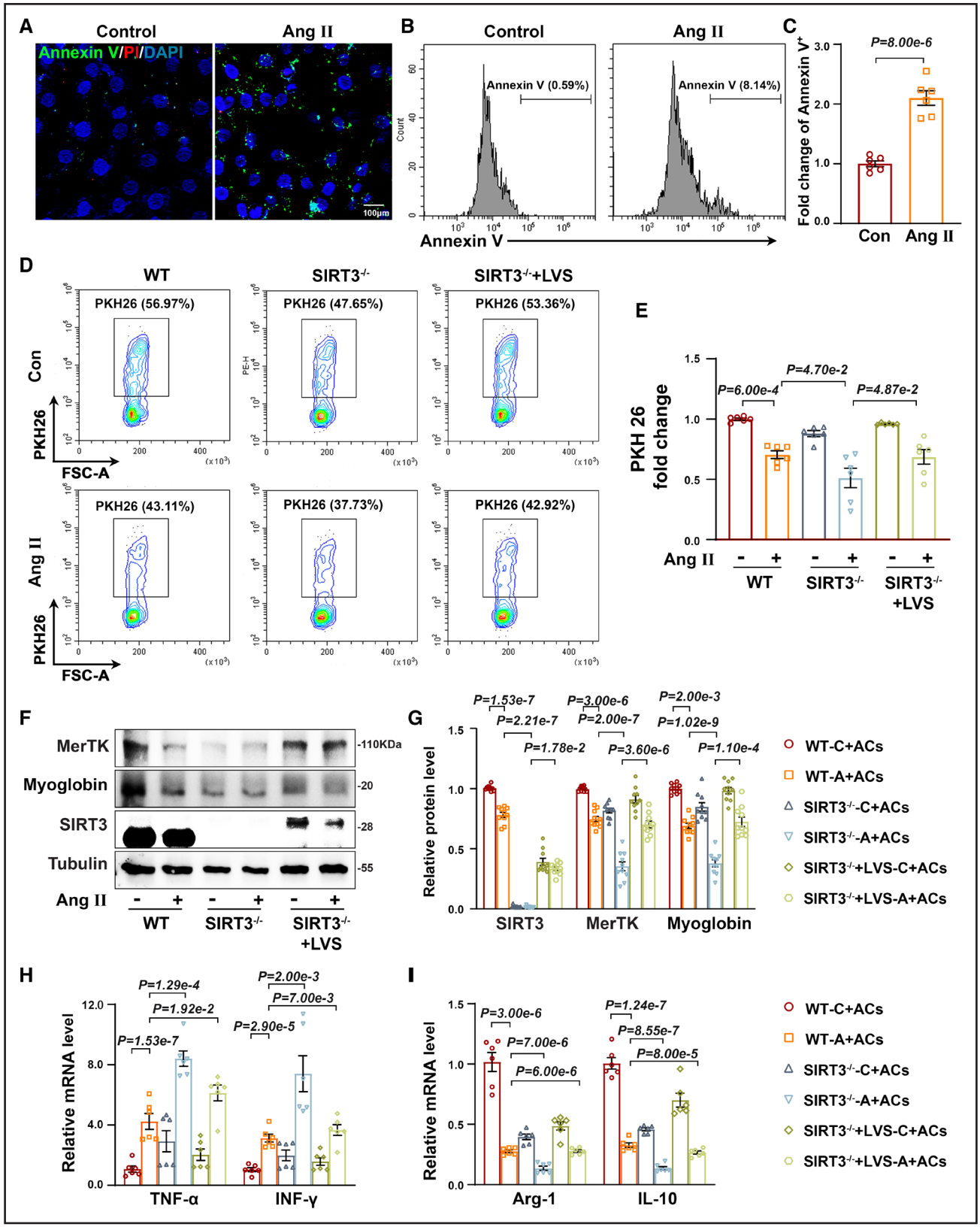

Figure 2. Macrophages take up apoptotic cell–derived myoglobin, which promotes proinflammatory macrophage activation. **A**, Mouse cardiac myocytes (MCMs) were treated with or without Ang II (angiotensin II) for 24 hours. Representative fluorescence micrographs of MCMs stained with annexin V (green), PI (red), and DAPI (blue). Scale bar, 100 μm. **B**, Representative flow cytometry images. **C**, Quantification of annexin V⁺ MCMs (n=6 independent experiments). Normal distribution was confirmed by the Shapiro-Wilk test. Significance of differences was examined by Student *t* test. **D**, PKH26-labeled apoptotic cardiomyocytes (ACs) cocultured with bone marrow–derived macrophages (*Continued*)

synthase), IFN-γ (interferon gamma), and IL (interleukin) 6 and reduced expression of the anti-inflammatory cytokines, such as Arg-1 (arginase-1), YM-1 (chitinase 3-like 3), IL-4, and IL-10 (Figure S1G).

Macrophages Phagocytose ACs to Promote Activation of Proinflammatory Macrophages

Annexin V was used to mask the externalized phosphatidylserine on the surface of ACs. Compared with the control group, Ang II significantly promoted mouse cardiac myocyte apoptosis (Figure 2A through 2C). We labeled UV-treated ACs (Figure S2A and S2B) with a membrane-integrating dye [PKH 26 (3H-Indolium,2-[3-(1,3-dihydro-3,3-dimethyl-1-tetradecyl-2H-indol-2-ylidene)-1-propen-1-yl]-1-docosyl-3,3-dimethyl-, iodide)] and cocultured them with bone marrow–derived macrophages (BMDMs) isolated from the WT and SIRT3 knockout mice. Ang II treatment significantly decreased the percentage of BMDMs engulfing ACs relative to the control group. The loss of SIRT3 accelerated Ang II–induced decline in phagocytosis, whereas reintroduction of lentivirus SIRT3 into SIRT3$^{-/-}$ cells increased the uptake of ACs (Figure 2D and 2E). After engulfing ACs, the protein levels of both SIRT3 and MerTK in Ang II–treated BMDMs were reduced, while myoglobin phagocytized by BMDMs was decreased in response to Ang II. This was further exacerbated in SIRT3$^{-/-}$ BMDMs. However, lentivirus SIRT3 reintroduced to SIRT3$^{-/-}$ cells increased the protein level of MerTK and elevated the uptake of myoglobin relative to SIRT3$^{-/-}$ cells (Figure 2F and 2G). As demonstrated in vivo, administration of Ang II upregulated the proinflammatory markers including TNF-α and IFN-γ and downregulated the anti-inflammatory markers such as Arg-1 and IL-10 in BMDMs. The loss of SIRT3 exacerbated the proinflammatory phenotype of Ang II–induced BMDMs. However, the reintroduction of SIRT3 to SIRT3-null BMDMs inhibited their proinflammatory activation (Figure 2H).

Macrophage Phagocytosis of ACs Induces Mitochondrial Iron Disorder

Phagocytic internalization of ACs increased the content of myoglobin, which can be broken by HO-1 into Fe^{2+}, biliverdin, and carbon monoxide. We next examined whether SIRT3 is involved in the regulation of mitochondrial iron metabolism. To this end, mitochondrial labile iron was measured in CD11b^{+} cells isolated from the myocardium using Mito-FerroGreen. We found that Ang II increased the Mito-FerroGreen fluorescence signal compared with that of the saline group, while the intracellular fluorescence became much stronger in the SIRT3 MKO group (Figure 3A and 3B).

For ex vivo efferocytosis assays, BMDMs were cocultured with ACs or hemin. After rinsing away the non-engulfed cells, we confirmed that the loss of SIRT3 promoted Ang II–induced mitochondrial labile iron; in contrast, reintroduction of SIRT3 reduced the level of mitochondrial labile iron (Figure 3C and 3D). The effects of hemin phagocytosis were similar to those of ACs phagocytosis (Figure 3E and 3F). Following hemin engulfment by BMDMs, Ang II administration increased the expression of the proinflammatory markers TNF-α and IFN-γ and decreased the expression of the anti-inflammatory markers Arg-1 and IL-10. Similarly, the absence of SIRT3 enhanced the proinflammatory activation of Ang II–induced BMDMs. In contrast, the reintroduction of SIRT3 to SIRT3-null BMDMs shifted their phenotype from proinflammatory to anti-inflammatory (Figure 3G).

To investigate whether mitochondrial iron overload results in impaired efferocytosis and a proinflammatory phenotype, we utilized the iron chelator deferoxamine to suppress intracellular free iron. Following hemin phagocytosis by M1920 cells, Ang II triggered elevated levels of mitochondrial labile iron, subsequently leading to decreased efferocytosis and proinflammatory activation of macrophages. Pretreatment with deferoxamine reduced mitochondrial labile iron (Figure 3H and 3I), enhanced efferocytosis (Figure 3J and 3K), and mitigated the proinflammatory activation of macrophages (Figure 3L). The expression of HO-1—an enzyme involved in myoglobin metabolism—was assessed in BMDMs. As shown in Figure S3A and S3B, the protein level of HO-1 was not affected by Ang II treatment over time. In contrast, hemin treatment led to a time-dependent increase in HO-1 protein level. Phagocytosis of ACs elevated the protein level of HO-1, which broke down myoglobin-associated heme into Fe^{2+}, bilirubin, and carbon monoxide. The upregulation of HO-1 compensated for the decrease in phagocytosed myoglobin, resulting in further mitochondrial iron

Figure 2 Continued. (BMDMs; wild type [WT], SIRT3 [sirtuin-3] knockout [SIRT3$^{-/-}$], and SIRT3$^{-/-}$+LVS [SIRT3 reconstruction]) for 1 hour with or without Ang II. Representative flow cytometry images of the proportion of BMDMs (F4/80^{+}) phagocytizing PKH26-labeled ACs. **E**, Quantification of BMDMs phagocytizing PKH26-labeled ACs (n=6 independent experiments). **F**, Representative Western blots of MerTK (c-Mer tyrosine kinase), myoglobin, and SIRT3 in BMDMs phagocytizing ACs. **G**, Quantitative analysis of SIRT3, MerTK, and myoglobin levels. The relative expression of each target protein was normalized to tubulin, and the fold change was calculated by comparing it to the control group (n=10 independent experiments). **H**, The mRNA expression levels of proinflammatory cytokines (**left**, TNF-α [tumor necrosis factor alpha] and IFN-γ [interferon gamma]) and anti-inflammatory cytokines (**right**, Arg-1 [arginase-1] and IL [interleukin]-10) in BMDMs phagocytizing ACs (n=6 independent experiments). Normal distribution was confirmed by the Shapiro-Wilk test. Significance of differences was examined by 2-way ANOVA followed by Tukey multiple comparison tests for **E**, **G**, and **H**. A indicates angiotensin II; C, control; LVS, lentivirus-Sirt3; and PKH 26, 3H-Indolium,2-[3-(1,3-dihydro-3,3-dimethyl-1-tetradecyl-2H-indol-2-ylidene)-1-propen-1-yl]-1-docosyl-3,3-dimethyl-, iodide.

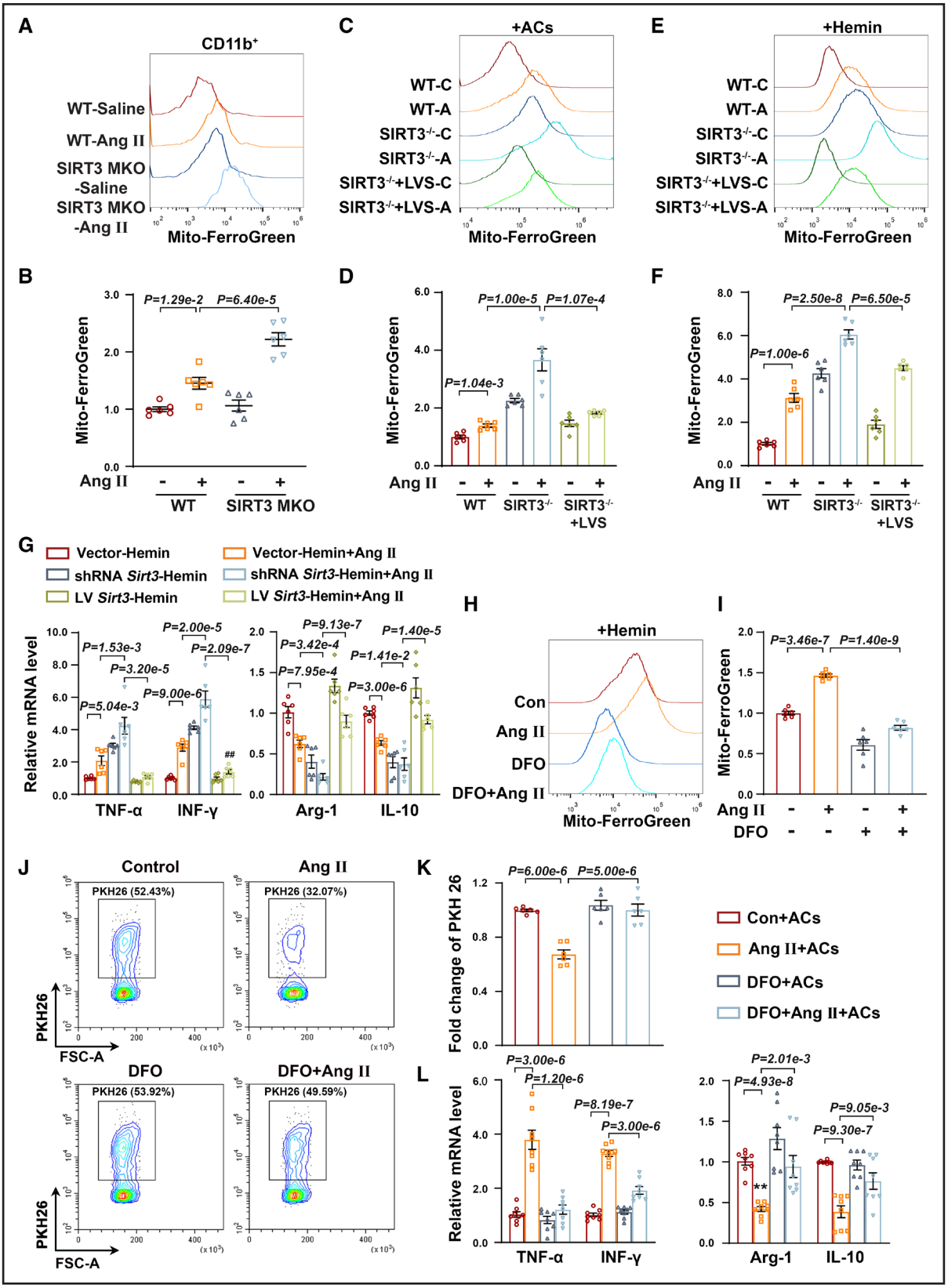

Figure 3. Phagocytosis of apoptotic cardiomyocytes (ACs) leads to mitochondrial iron metabolism dysfunction in macrophages. **A**, Representative flow cytometry images of CD11b+ cells purified from the wild-type (WT) and myeloid SIRT3 (sirtuin-3) knockout (SIRT3 MKO) mice myocardium stained with Mito-FerroGreen. **B**, Fluorescence intensity of Mito-FerroGreen in CD11b+ cells (n=6 mice per group). Statistical analysis was performed by Kruskal-Wallis test followed by Dunn multiple comparisons tests. **C**, Representative flow cytometry images of bone marrow–derived macrophages (BMDMs; WT, SIRT3 knockout [SIRT3$^{-/-}$], and SIRT3$^{-/-}$+LVS [SIRT3 reconstruction]) (*Continued*)

accumulation (Figure S3C). We examined the impact of zinc protoporphyrin IX—an HO-1 inhibitor—on BMDMs following their phagocytosis of ACs. Our results indicate that zinc protoporphyrin IX led to a decrease in Mito-FerroGreen signaling (Figure S3D and S3E).

SIRT3 Interacts With FXN

To determine the downstream target of SIRT3-mediated mitochondrial labile iron, we used acetyl-lysine antibody affinity purification and mass spectrometry to identify differences in acetylated proteins between WT and SIRT3$^{-/-}$ BMDMs. A summary of the SIRT3-targeted acetylproteome, including quantifiable acetyl-lysines and corresponding proteins targeted for deacetylation, is provided in Figure S4A. Additionally, Figure S4B through S4D displays the acetylation abundance of SIRT3-targeted lysines on the subunits of proteins involved in the electron transport chain, reactive oxygen species detoxification, and the tricarboxylic acid cycle.

According to mass spectrometry data, the acetylation level of FXN^{K189} was upregulated 2-fold in SIRT3$^{-/-}$ cells (Figure 4A). FXN is a mitochondrial protein that promotes the synthesis of ISCs and facilitates their introduction into enzymes containing ISCs, including complexes I, II, and III. By comparing the murine FXN amino acid sequence between ≈150 and 207 nt with that of different species, including *Homo sapiens* (human), *Mus musculus* (house mouse), *Canis lupus familiaris* (domestic dogs), *Equus asinus* (donkeys), *Drosophila hydei*, *Necator americanus*, and *Pluteust cervinus*, we found that K189 is evolutionarily conserved, despite a modest shift in sequence position between the species (K192 in *Homo sapiens*, K193 in *Canis lupus familiaris*, K160 in *Equus asinus*, K167 in *Drosophila hydei*, K139 in *Necator americanus*, and K101 in *Pluteust cervinus*; Figure 4B).

To verify the results obtained by mass spectrometry, we examined the endogenous and exogenous interactions between SIRT3 and FXN in M1920 cells. Proteins were coimmunoprecipitated with either anti-FXN (Figure 4C) or anti-SIRT3 (Figure 4D), and the pull-down samples were immunoblotted with SIRT3 or FXN antibodies. HA (hemagglutinin) tagged-SIRT3 or Flag-FXN was transfected into M1920 cells, and the expression of FXN and SIRT3 was detected after the extracts were immunoprecipitated with either Flag-conjugated beads (Figure 4E) or HA beads (Figure 4F), indicating an interaction between SIRT3 or FXN.

Acetylation of FXN was significantly enhanced in M1920 cells treated with the deacetylase inhibitor nicotinamide, which suggests that acetylation is a major posttranslational modification of FXN (Figure 4G). An antibody that specifically recognizes K189-acetylated FXN—produced by immunizing rabbits with the K189-acetylated peptide (RELTK[Ac]ALNTKLDLC)—was used to detect K189 acetylation in M1920 cells infected with *shRNA-Sirt3* or *LV-Sirt3* lentivirus. Ang II–induced Ace-FXN^{K189} levels were promoted by the ablation of SIRT3 and reduced by SIRT3 overexpression (Figure 4H and 4I), indicating that SIRT3 deacetylated FXN at K189. The myocardial sections were costained with CD68 and Ace-FXN^{K189} using immunofluorescence. Ang II treatment of the mice increased the yellow signal of Ace-FXN^{K189} colocalized with CD68^{+} macrophages. The number of Ace-FXN^{K189}–associated CD68^{+} cells was further elevated in the SIRT3 MKO group (Figure S4E).

To determine whether acetylation of K189 mediates FXN activity, 293T cells were transfected with *Flag-Fxn^{WT}*, *Flag-Fxn^{K189R}*, and *Flag-Fxn^{K189Q}*, and the activity and expression of complex I were detected. *Flag-Fxn^{K189R}* transfection increased the activity and expression of complex I, whereas *Flag-Fxn^{K189Q}* transfection showed the opposite effect (Figure 4J through 4L), further confirming that K189 acetylation reduces FXN activity.

Deacetylated FXN Elevates the Efferocytosis Capacity

Next, to examine the role of FXN in efferocytosis and macrophage phenotype, we examined the gain and loss of FXN expression in M1920 cells. Knockdown of FXN aggravated Ang II–induced high levels of mitochondrial labile iron (Figure 5A and 5B) and shifted

Figure 3 Continued. phagocytizing ACs stained with Mito-FerroGreen. **D**, Fluorescence intensity of Mito-FerroGreen in BMDMs (n=6 independent experiments). **E**, BMDMs (WT, SIRT3$^{-/-}$, and SIRT3$^{-/-}$+LVS) phagocyted hemin for 1 hour with or without Ang II (angiotensin II). Representative flow cytometry images of BMDMs stained with Mito-FerroGreen. **F**, Fluorescence intensity of Mito-FerroGreen in BMDMs (n=6 independent experiments). **G**, The mRNA expression levels of proinflammatory genes (**left**, TNF-α [tumor necrosis factor alpha] and IFN-γ [interferon gamma]) and anti-inflammatory genes (**right**, Arg-1 [arginase-1] and IL [interleukin]-10) in M1920 cells infected with shRNA-*Sirt3*, LV-*Sirt3*, or vector and phagocyting hemin (n=6 independent experiments). **H**, BMDMs were preincubated with deferoxamine (DFO) for 1 hour, followed by treatment with Ang II. Representative flow cytometry images of DFO-treated BMDMs stained with Mito-FerroGreen. **I**, Fluorescence intensity of Mito-FerroGreen in BMDMs (n=6 independent experiments). **J**, Representative flow cytometry images of the proportion of BMDMs phagocytizing PKH26-labeled ACs. **K**, Quantification of BMDMs phagocytizing PKH26-labeled ACs (n=6 independent experiments). **L**, The mRNA expression levels of proinflammatory genes (**left**, TNF-α and IFN-γ) and anti-inflammatory genes (**right**, Arg-1 and IL-10) in BMDMs treated with DFO (n=6 independent experiments). Normal distribution was confirmed by the Shapiro-Wilk test. Significance of differences was examined by 2-way ANOVA followed by Tukey multiple comparisons tests for **D**, **F**, **G**, **I**, **K**, and **L**. A indicates angiotensin II; C, control; CD, cluster of differentiation; LVS, lentivirus-Sirt3; and PKH 26, 3H-Indolium,2-[3-(1,3-dihydro-3,3-dimethyl-1-tetradecyl-2H-indol-2-ylidene)-1-propen-1-yl]-1-docosyl-3,3-dimethyl-, iodide.

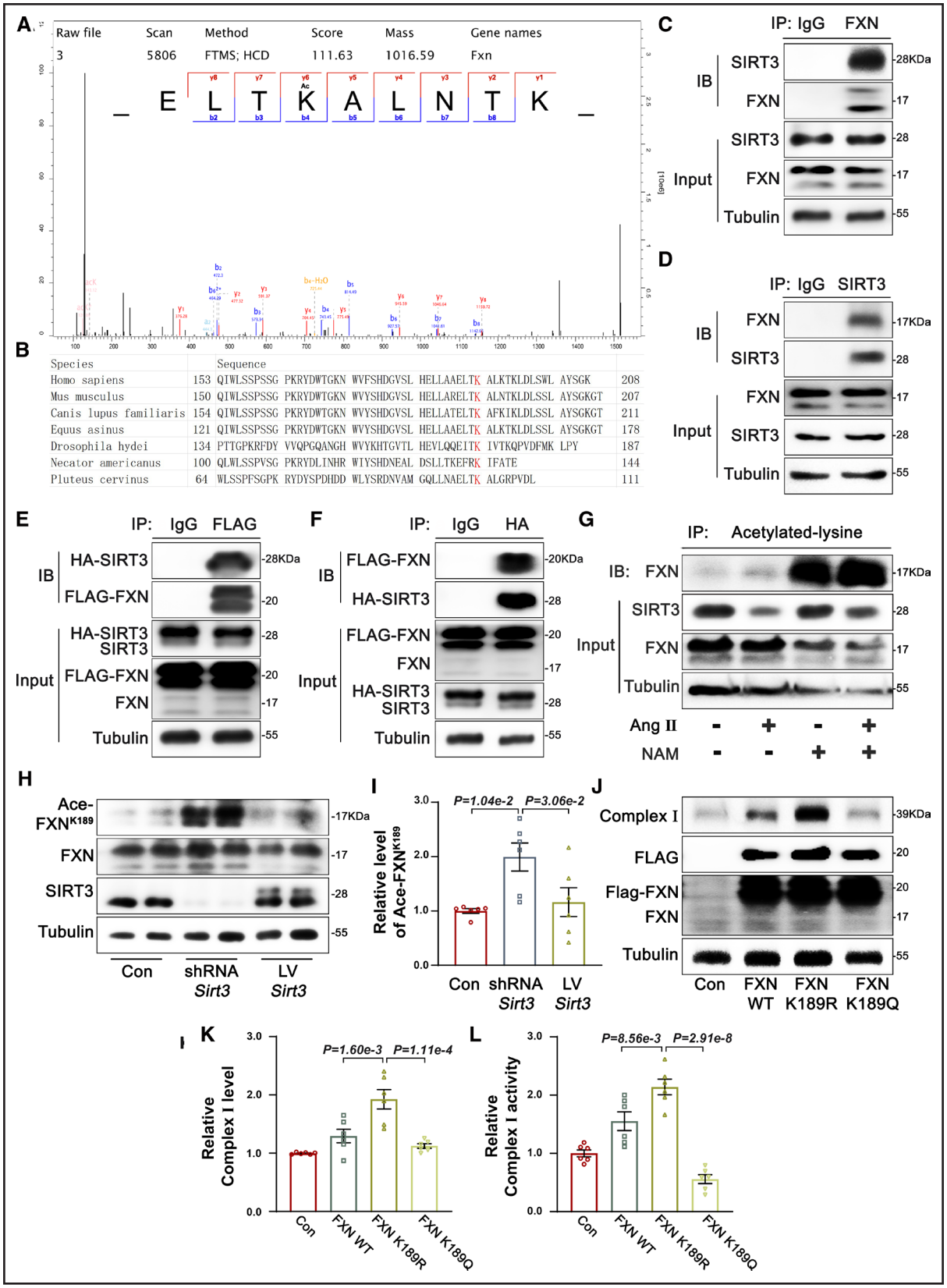

Figure 4. Sirt3 (sirtuin-3) interacts with FXN (frataxin).
A, The mass spectrum of FXN acetylation sites in SIRT3 knockout (SIRT3 MKO) mice compared with wild-type (WT) mice. **B**, The amino acid sequence of FXN between ≈150 and 207 nt across species. **C**, Western blot of SIRT3 level following immunoprecipitation with anti-FXN antibody in M1920 cells. **D**, Western blot of FXN level following immunoprecipitation with anti-SIRT3 antibody in M1920 cells. **E**, M1920 cells were transfected with HA (hemagglutinin)-SIRT3 and Flag-FXN. Western blot of SIRT3 level following immunoprecipitation with anti-Flag antibody. **F**, (*Continued*)

M1920 cells toward the proinflammatory phenotype (Figure 5C). In contrast, overexpression of FXN in M1920 cells reduced mitochondrial labile iron levels and the expression of proinflammatory cytokines (Figure 5A through 5C).

To explore whether acetylated FXN is involved in Ang II–induced impairment of efferocytosis and proinflammatory phenotype, we generated an FXN^{K189R} mutant mouse model using CRISPR/Cas9 (clustered regularly interspaced short palindromic repeats/CRISPR-associated protein 9) technology. This mutation of lysine to arginine mimics FXN deacetylation. BMDMs isolated from the WT and FXN^{K189R} mice were stimulated with or without Ang II for 24 hours and then incubated with PKH26-labeled ACs. The percentage of BMDMs engulfing ACs after Ang II treatment was significantly reduced relative to that in the control group. Mutation of FXN elevated Ang II–induced hypophagocytosis, followed by increased MerTK protein levels and detectable myoglobin content in BMDMs (Figure 5D through 5G). Although mutation of FXN elevated myoglobin uptake, flow cytometry illustrated that Mito-FerroGreen signals of FXN^{K189R} BMDMs were much lower than those in the WT group, confirming that the K189 acetylation level determines FXN activity (Figure 5H and 5I). As expected, Ang II was able to induce the proinflammatory phenotype, which was partially abrogated by the FXN^{K189R} mutation (Figure 5J). These data further confirmed that deacetylation of FXN^{K189R} restored the efferocytosis capacity and inflammation resolution.

SIRT3-FXN Axis Regulates Efferocytosis and Proinflammatory Macrophage Activation via the NF-κB Pathway

Considering that mitochondrial iron deposition triggers free radical production via the Fenton reaction, we next measured oxidative stress by examining the levels of lipid peroxides, which are major products of lipid peroxidation. After phagocytosis of ACs, liperfluo signals were significantly increased in the WT–Ang II group and further strengthened in the SIRT3$^{-/-}$–Ang II group, whereas reintroduction of SIRT3 reduced the level of lipid peroxides (Figure 6A and 6B). Similarly, FXN^{K189R} BMDMs quenched Ang II–induced fluorescence (Figure 6C and 6D). NF-κB (nuclear factor kappa B) is an oxidative stress–responsive transcription factor. Not only is it involved in regulating the expression of various proinflammatory cytokines but it also plays a role in efferocytosis. NF-κB is a heterodimer composed of 50 kDa (p50) and 65 kDa (p65) subunits in complex with inhibitory IκB proteins. In line with the level of lipid peroxides, Ang II–induced phosphorylation of IκBα (nuclear factor of kappa light polypeptide gene enhancer in B-cells inhibitor, alpha) and NF-κB p65 was intensified in SIRT3$^{-/-}$ BMDMs and abridged in FXN^{K189R} BMDMs (Figure 6E and 6F). Mitoquinone is a mitochondria-targeted antioxidant that specifically scavenges reactive oxygen species in the mitochondria. We found that pretreatment with mitoquinone inhibited Ang II–induced activation of IκBα and NF-κB p65 (Figure 6G and 6H). To verify the involvement of the NF-κB pathway in efferocytosis and proinflammatory macrophage activation, we used a metal chelator and the radical-scavenging antioxidant pyrrolidine dithiocarbamate. On one hand, pyrrolidine dithiocarbamate specifically inhibited NF-κB activation (Figure 6I); on the other hand, it reversed MerTK expression and attenuated proinflammatory macrophage activation induced by Ang II treatment (Figure 6J through 6L).

FXN Deacetylation Improves Macrophage Mitochondrial Iron Homeostasis and Efferocytosis

To further examine the role of deacetylated FXN in vivo, WT and FXN^{K189R} mice were exposed to Ang II for 7 days. To verify the acetylation levels of FXN in the FXN^{K189R} mouse model, we isolated BMDMs from both the WT and the FXN^{K189R} mice that had received either saline or Ang II infusion for 7 days. Using acetylation-specific antibodies, we found that FXN acetylation levels were increased in Ang II–treated WT mice but decreased in FXN^{K189R} mice (Figure S5A). Blood pressure similarly increased in WT and FXN^{K189R} mice during Ang II infusion (Figure S5B). FXN^{K189R} mice were resistant to Ang II–induced cardiac fibrosis, which was robust in the WT group (Figure 7A). FXN^{K189R} hearts exhibited a significantly decreased number of TUNEL^{+} cardiomyocytes relative to the control (Figure 7B and 7C). Although acetyl-defective FXN did not alter the macrophage populations induced by Ang II (Figure S6A and S6B), MerTK protein levels were increased in both CCR2^{+} and CCR2^{-} macrophages (Figure 7D

Figure 4 Continued. Western blot of FXN level following immunoprecipitation with anti-HA. **G**, Representative Western blot of acetylated FXN in M1920 cells treated with nicotinamide (NAM). **H**, Representative Western blots of acetylated FXN lysine 189 (FXN K189-Ac) in M1920 cells infected with shRNA *Sirt3* or LV-*Sirt3*. **I**, Quantitative analysis of FXN K189-Ac levels in M1920 cells (n=6 independent experiments). **J**, Representative Western blots of complex I in 293T cells transfected with Flag-*Fxn*^{WT}, Flag-*Fxn*^{189KR}, and Flag-*Fxn*^{189KQ}. **K**, Quantitative analysis of complex I in 293T cells (n=6 independent experiments). **L**, Complex I activity of 293T cells transfected with Flag-*Fxn*^{WT}, Flag-*Fxn*^{189KR}, and Flag-*Fxn*^{189KQ} (n=6 independent experiments). The relative expression of each target protein was normalized to tubulin, and the fold change was calculated by comparing it to the control group. Significance of differences was examined by 1-way ANOVA followed by Tukey multiple comparisons tests for **I**, **K**, and **L**. F-FXN indicates Flag tagged-FXN; H-SIRT3, HA tagged-SIRT3; IB, immunoblot; LV-*Sirt3*, lentivirus-*Sirt3*; and shRNA *Sirt3*, short hairpin RNA *Sirt3* lentivirus.

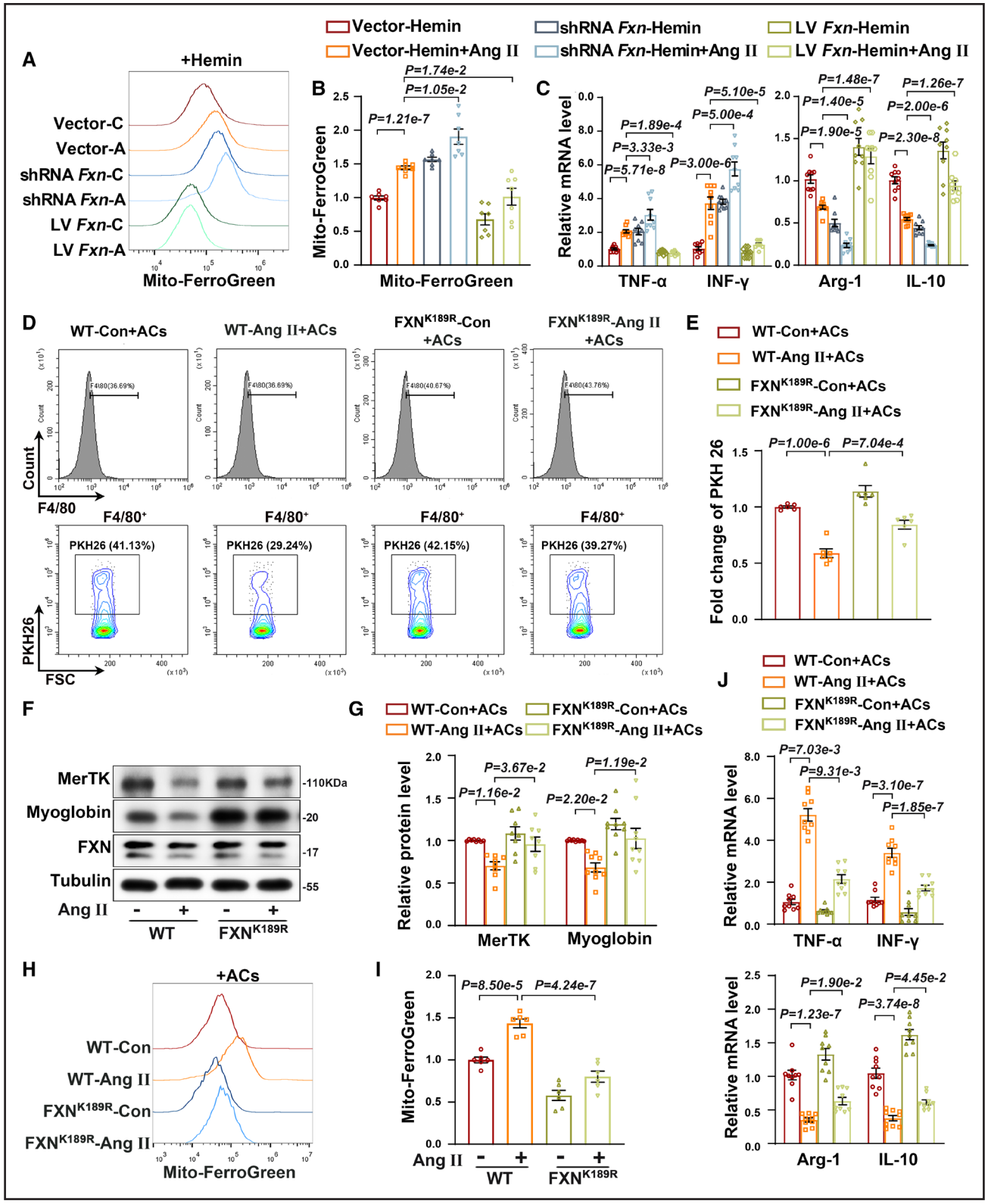

Figure 5. FXN (frataxin) restores the efferocytosis capacity and macrophage phenotype.
A, M1920 cells were infected with short hairpin RNA (shRNA)–*Fxn*, lentivirus (LV)-*Fxn*, or empty vector and phagocyted hemin. Representative flow cytometry images of M1920 cells stained with Mito-FerroGreen. **B**, Fluorescence intensity of Mito-FerroGreen in M1920 cells (n=7 independent experiments). **C**, The mRNA expression levels of proinflammatory genes (**left**, TNF-α [tumor necrosis factor alpha] and IFN-γ [interferon gamma]) and anti-inflammatory genes (**right**, Arg-1 [arginase-1] and IL [interleukin]-10) in M1920 cells infected with shRNA-*Fxn*, LV-*Fxn*, or empty vector (n=9 independent experiments). **D**, PKH26-labeled apoptotic cardiomyocytes (ACs) cocultured with bone marrow–derived macrophages (BMDMs) isolated from wild-type (WT) and FXN mutation (FXN^{K189R}) mice for 1 hour with or without (*Continued*)

and 7E). CD11b$^+$ cells isolated from FXN^{K189R} mice showed elevated MerTK protein levels (Figure 7F and 7G), as well as reduced expression of proinflammatory cytokines and increased expression of anti-inflammatory cytokines (Figure 7H). These results suggest that FXN^{K189R} deacetylation enhances efferocytosis and promotes an anti-inflammatory phenotype in cardiac macrophages, thereby contributing to the resolution of cardiac inflammation.

DISCUSSION

Targeting the clearance of ACs by efferocytosis is important for the resolution of cardiac inflammation.[22] However, the link between efferocytosis and metabolic rewiring remains poorly understood. In this study, we showed that myocardial degeneration depends on the ability of myocardium-infiltrating macrophages to process iron. The key findings of the present study are as follows: (1) SIRT3-deficient macrophages impair AC clearance; (2) acetylated FXN disrupts mitochondrial iron homeostasis; (3) engulfment of ACs elevates macrophage mitochondrial labile iron; and (4) mitochondrial iron disorder leads to defective efferocytosis and proinflammatory macrophage activation.

Effective efferocytosis depends on the major signaling programs. Namely, exposure of phosphatidylserine on the surface of ACs leads to the activation of MerTK on macrophages, which triggers engulfment of ACs and subsequent activation of the anti-inflammatory macrophage phenotype.[23] In contrast, defective efferocytosis induces secondary necrosis of ACs and results in proinflammatory macrophage activation.[24] Cardiomyocytes are terminally differentiated cells that are susceptible to defective efferocytosis.[25,26] The current study showed that Ang II infusion increased the recruitment of monocyte-derived macrophages and expansion of resident macrophages, accompanied by decreased SIRT3 activity. Although SIRT3 ablation did not have a significant effect on the composition of recruited or resident macrophages, it aggravated the decrease in MerTK expression in both CCR2$^+$ and CCR2$^-$ macrophages, and they displayed a proinflammatory phenotype by secreting cytokines such as TNF-α and IL-6. Of note, the increased accumulation of ACs coincided with a reduced index of efferocytosis receptor MerTK. Overexpression of SIRT3 rescued defective efferocytosis under hypertensive conditions, thereby improving the anti-inflammatory macrophage phenotype. These data indicate that SIRT3 improves macrophage efferocytosis.

Macrophages are specialized phagocytic cells that efficiently engulf and remove dying or dead cells. The metabolic substrates derived from apoptotic cells, also known as efferocytosis catabolism, have the potential to directly influence macrophage phenotype. Several studies have demonstrated that the metabolism of AC-derived metabolites—including fatty acids,[4] nucleotides,[27] amino acids,[28] vitamins,[29] cholesterol,[30] and arginine[31]—from efferocytosis augments subsequent rounds of efferocytosis and supports anti-inflammatory effects. These results demonstrated that AC-derived metabolites could indeed be reused as substrates for macrophage reprogramming. However, the efferocytosis capacity and macrophage phenotype depend on mitochondrial function. Impairments in myeloid mitochondrial complex III result in IL-10–dependent myocardial injury and defects in resolution of inflammation.[4] Myeloid-specific deletion of mitochondrial complex I reproduces the proinflammatory metabolic profile, glycolysis, in macrophages, thereby leading to impaired efferocytosis and lower expression of anti-inflammatory cytokines.[32] Deficiencies in Arg-1 or ornithine decarboxylase (ODC) reduce myeloid cells constant efferocytosis and the resolution of atherosclerosis.[31] Disruption of mitochondrial metabolic function has been shown to contribute to defective efferocytosis.[30,33]

Considering that macrophages are strong candidates for sustaining iron homeostatic functions, previous studies have suggested a link between Fe^{2+} and efferocytosis.[34] Mitochondrial iron homeostasis is regulated by the dynamic balance between mitochondrial iron uptake, iron storage, and iron utilization.[35] In line with recent literature, we found that Ang II treatment increased mitochondrial labile iron in macrophages. FXN is an important and uncharacterized mitochondrial protein that regulates iron utilization and iron chaperone.[36] In humans, mutations that affect FXN expression and function result in Friedreich ataxia, a progressive neurological and cardiac degeneration disorder.[37] The genetic basis for this deficiency is an expansion of a GAA (guanine-adenine-adenine). repeat, which hinders the transcription of the *Fxn* gene.[38,39] However, the regulatory factors that influence FXN expression are not sufficiently known. Wagner et al[17] first reported that highly acetylated FXN negatively correlated with SIRT3 expression levels. We further found that mitochondrial SIRT3 deacetylated

Figure 5 Continued. Ang II (angiotensin II). Representative flow cytometry images of the proportion of BMDMs phagocytizing PKH26-labeled ACs. **E**, Quantification of BMDMs phagocytizing PKH26-labeled ACs (n=6 independent experiments). **F**, Representative Western blots of MerTK (c-Mer tyrosine kinase), myoglobin, and FXN in BMDMs phagocytizing ACs. The relative expression of each target protein was normalized to tubulin, and the fold change was calculated by comparing it to the control group. **G**, Quantitative analysis of MerTK and myoglobin levels (n=9 independent experiments). **H**, Representative flow cytometry images of BMDMs stained with Mito-FerroGreen. **I**, Fluorescence intensity of Mito-FerroGreen in BMDMs (n=6 independent experiments). **J**, The mRNA expression levels of proinflammatory genes (**top**, TNF-α and IFN-γ) and anti-inflammatory genes (**bottom**, Arg-1 and IL-10) in BMDMs phagocytizing ACs (n=9 independent experiments). Significance of differences was examined by 2-way ANOVA followed by Tukey multiple comparisons tests for **B**, **C**, **E**, **G**, **I**, and **J**. PKH 26 indicates 3H-Indolium,2-[3-(1,3-dihydro-3,3-dimethyl-1-tetradecyl-2H-indol-2-ylidene)-1-propen-1-yl]-1-docosyl-3,3-dimethyl-, iodide.

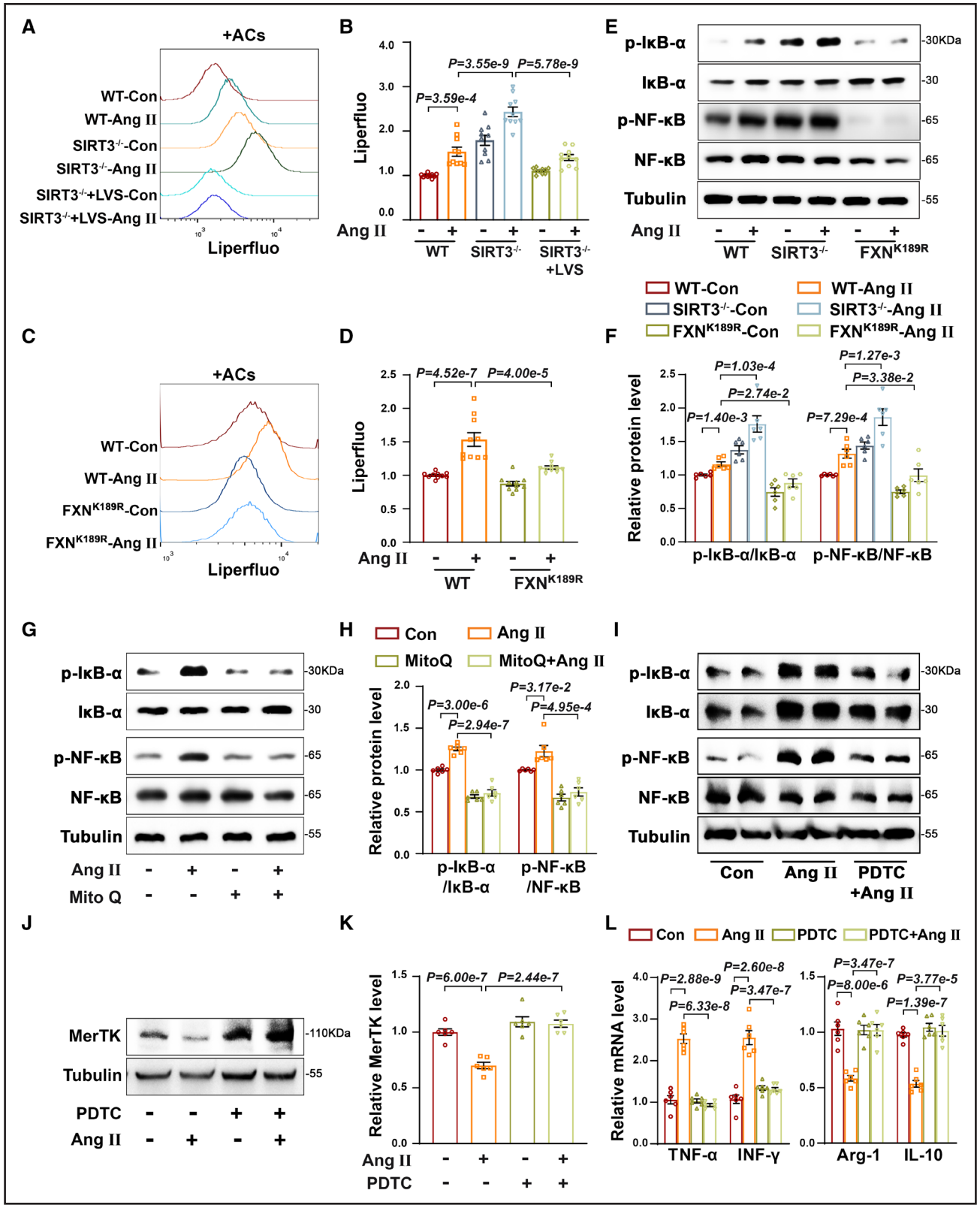

Figure 6. The SIRT3 (sirtuin-3)-FXN (frataxin) axis regulates efferocytosis via NF-κB (nuclear factor kappa B).
A, Representative flow cytometry images of bone marrow–derived macrophages (BMDMs; wild type [WT], SIRT3$^{-/-}$, and SIRT3$^{-/-}$+LVS) phagocytizing apoptotic cardiomyocytes (ACs) stained with liperfluo. **B**, Fluorescence intensity of liperfluo in BMDMs (n=10 independent experiments). **C**, Representative flow cytometry images of BMDMs (WT and FXN^{K189R}) phagocytizing ACs stained with liperfluo. **D**, Fluorescence intensity of liperfluo in BMDMs (n=10 independent experiments). **E**, Representative Western blots of phospho-IκB-alpha (p-IκB-α), IκB-α, phospho-NF-κB (p-NF-κB), and NF-κB in BMDMs isolated from WT, SIRT3$^{-/-}$, and Fxn^{K189R} treated with or without Ang II (*Continued*)

the K189 site of FXN, which determines FXN activity, while hyperacetylated FXN reduced ISC formation, as evidenced by the low activity and protein levels of complex I. The fine-tuning effect of K189 deacetylation on FXN activity decreased mitochondrial iron overload and lipid peroxidation, which correlated with macrophage efferocytosis and phenotype. Ang II inhibited SIRT3 expression and promoted hyperacetylation of FXN lysine 189, and hyperacetylation modifications of FXN were involved in mitochondrial iron metabolism.

The uptake of apoptotic cells is a key function of macrophages, which is controlled by cellular metabolism.[40] After engulfing ACs, myoglobin was detected in infiltrating macrophages, paralleling the high levels of mitochondrial labile iron. The expression of HO-1, an inducible isoform of the heme-degrading enzyme, is promoted by various stress stimuli. In the present study, although Ang II alone did not have a significant effect on HO-1 protein levels, phagocytosis of hemin produced a time-dependent effect on HO-1 protein levels. These findings explain the high levels of mitochondrial labile iron in macrophages despite the decrease in phagocytic myoglobin content. Therefore, we speculated that phagocytic internalization of ACs liberates myoglobin-derived Fe^{2+} to deteriorate mitochondrial iron disorders. Next, we used the intracellular iron chelator deferoxamine to prevent iron uptake from transferrin. As expected, deferoxamine pretreatment not only decreased mitochondrial labile iron but also increased efferocytosis. This finding confirmed that mitochondrial iron disorder compromises the integrated metabolic response of macrophages.

Another aspect of efferocytosis catabolism is that metabolic substrates from ACs may directly influence macrophage phenotype. Three recent studies have revealed that AC-derived cholesterol, fatty acids, and amino acids can act as major substrates for mitochondrial metabolism to facilitate the production of anti-inflammatory cytokines.[4,31,41] Mitochondrial metabolism has a huge impact on immune cell function, and compromised mitochondrial fission reduces macrophage phagocytic capacity and expands inflammation.[33] Moreover, defects in the mitochondrial electron transport chain may inhibit the secretion of anti-inflammatory IL-10. We demonstrated that engulfment of ACs or hemin by SIRT3- or FXN-deficient BMDMs and M1920 cells increased mitochondrial labile iron and the accumulation of lipid peroxides. In contrast, reconstruction of SIRT3 or FXN^{K189R} (mutation of K189 from lysine to arginine) attenuated Ang II–induced mitochondrial iron disorder and proinflammatory macrophage phenotype. Excessive mitochondrial labile iron can promote reactive oxygen species production. Therefore, deferoxamine was applied to inhibit the accumulation of labile iron and reactive oxygen species in the mitochondria, thereby promoting the anti-inflammatory macrophage phenotype. Mitoquinone—a scavenger of mitochondrial lipid peroxidation induced by Fenton reaction—had the same effects. Collectively, these data suggest that Ang II induces macrophage phenotype alteration through oxidative stress caused by mitochondrial iron overload.

Recent research has revealed that NF-κB and its inhibitory protein IκBα are downstream targets in the regulation of cardiac inflammation during hypertrophic remodeling. Our immunoblots showed that SIRT3 deficiency intensified Ang II–stimulated IκBα degradation and NF-κB p65 activation, which was reversed by the reconstruction of SIRT3 or FXN^{K189R} macrophages. Furthermore, pyrrolidine dithiocarbamate—a potent inhibitor of NF-κB—attenuated Ang II–induced inhibition of efferocytosis and MerTK expression. These effects were similar to those of the reconstruction of SIRT3 and FXN^{K189R} macrophages. Our findings are consistent with a previous report that NF-κB p65 binds to the BS2 region of the MerTK promoter and inhibits MertK-mediated efferocytosis.[42] In addition, blocking the activation of NF-κB signaling reduces the proinflammatory phenotype. Our data suggest that IκBα/NF-κB signaling is a common pathway that regulates macrophage efferocytosis and phenotype.

Collectively, Ang II inhibits SIRT3 expression and promotes the hyperacetylation of FXN lysine 189, and acetylation modification of FXN leads to mitochondrial iron overload. The heme-derived metabolites of macrophage phagocytic internalization of ACs can further exacerbate mitochondrial labile iron and lipid peroxidation. Activation of the redox-sensitive transcription factor NF-κB signaling pathway contributes to defective efferocytosis and proinflammatory macrophage activation. FXN knock-in mice bearing an acetylation-defective lysine to arginine (K189R) mutation show enhanced macrophage efferocytosis, improved cardiac inflammation, and decreased fibrosis.

Figure 6 Continued. (angiotensin II) for 15 minutes. **F**, Quantitative analysis of p-IκB-α and p-NF-κB levels (n=6 independent experiments). **G**, BMDMs were preincubated with mitoquinone (MitoQ) for 1 hour, followed by Ang II treatment for 15 minutes. Representative Western blots of p-IκB-α, IκB-α, p-NF-κB, and NF-κB in BMDMs. **H**, Quantitative analysis of p-IκB-α and p-NF-κB levels (n=6 independent experiments). **I**, Representative Western blots of p-IκB-α, IκB-α, p-NF-κB, and NF-κB in M1920 cells treated with pyrrolidine dithiocarbamate (PDTC) for 1 hour. **J**, Representative Western blots of MerTK (c-Mer tyrosine kinase) in M1920 cells treated with PDTC. **K**, Quantitative analysis of MerTK (n=6 independent experiments). The relative expression of each target protein was normalized to tubulin, and the fold change was calculated by comparing it to the control group. **L**, The mRNA expression levels of proinflammatory genes (**left**, TNF-α [tumor necrosis factor alpha] and IFN-γ [interferon gamma]) and anti-inflammatory genes (**right**, Arg-1 [arginase-1] and IL [interleukin]-10) in M1920 cells treated with PDTC (n=6 independent experiments). Data are shown as mean±SEM. Normal distribution was confirmed by the Shapiro-Wilk test. Significance of differences was examined by 2-way ANOVA followed by Tukey multiple comparisons tests for **B**, **D**, **F**, **H**, **K**, and **L**.

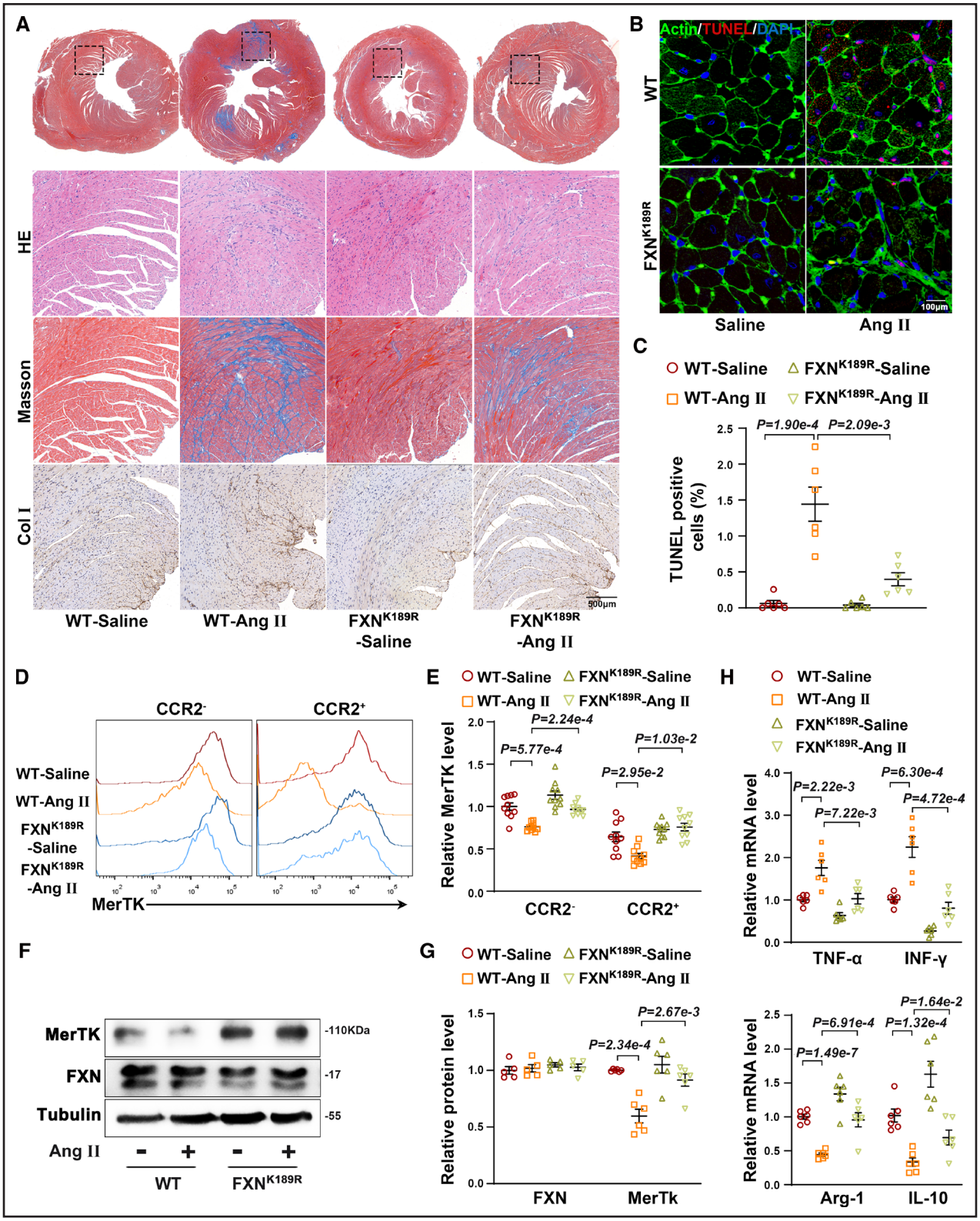

Figure 7. FXN (frataxin) deacetylation improves macrophage mitochondrial iron homeostasis and efferocytosis.
A, Eight-week-old wild-type (WT) and FXN^{K189R} mice were given 1500 ng·kg^{-1}·min^{-1} of Ang II (angiotensin II) or saline for 7 days. Representative H&E, Masson trichrome staining, and collagen I immunocytochemistry staining of the mice hearts. Scale bar, 500 μm. **B**, Representative fluorescence micrographs of the sections of the heart labeled with TUNEL (terminal deoxynucleotidyl transferase dUTP nick-end labeling; red), cardiomyocytic actin (green), and DAPI (blue). Scale bar, 100 μm. **C**, Number of TUNEL-positive nuclei presented as the percentage of the total number of nuclei in the sections of the heart (n=6 mice per group). Statistical analysis was performed by the Kruskal-Wallis test followed by Dunn multiple comparisons tests. **D**, Representative flow cytometry images of MerTK (c-Mer tyrosine kinase) expression on gated (*Continued*)

Figure 7 Continued. CD11b$^+$CD64$^+$CCR2 (C-C motif chemokine receptor 2)$^-$ or CD11b$^+$CD64$^+$CCR2$^+$ cells in the heart. **E**, Representative fluorescence intensity of MerTK in CD11b$^+$CD64$^+$CCR2$^-$ or CD11b$^+$CD64$^+$CCR2$^+$ cells in the heart (n=10 mice per group). Significance of differences was examined by 2-way ANOVA followed by Tukey multiple comparisons tests. **F**, Representative Western blots of MerTK and FXN in CD11b$^+$ cells isolated from WT and FXN^{K189R} mice. **G**, Quantitative analysis of MerTK and FXN levels (n=6 mice per group). Statistical analysis was performed by Kruskal-Wallis test followed by Dunn multiple comparisons tests. **H**, The mRNA expression levels of proinflammatory genes (**top**, TNF-α [tumor necrosis factor alpha] and IFN-γ [interferon gamma]) and anti-inflammatory genes (**bottom**, Arg-1 [arginase-1] and IL [interleukin]-10) in CD11b$^+$ cells separated from the hearts of WT and FXN^{K189R} mice using quantitative real-time polymerase chain reaction (n=6 mice per group). Statistical analysis was performed by Kruskal-Wallis test followed by Dunn multiple comparisons tests. CD indicates cluster of differentiation.

ARTICLE INFORMATION

Received June 12, 2023; revision received August 9, 2023; accepted August 11, 2023.

Affiliations

Department of Cardiovascular Medicine, State Key Laboratory of Medical Genomics, Shanghai Key Laboratory of Hypertension, Shanghai Institute of Hypertension, Ruijin Hospital (J.G., C.H., L.K., T.W., W.S.) and Department of Emergency, Shanghai Ninth People's Hospital (W.Z.), Shanghai Jiao Tong University School of Medicine, China. Key Laboratory of State General Administration of Sport, Shanghai Research Institute of Sports Science, China (M.S.).

Acknowledgments

The authors would like to thank Jinjie PTM Biolab Co, Ltd (Hangzhou, China), for performing the mass spectrometry analysis.

Sources of Funding

This study was supported by the grants from the National Natural Science Foundation of China (No. 82170248 and 81970235), the Natural Science Foundation of Shanghai (20ZR1454300 and 19ZR1443200), and the Natural Science Foundation of Tibet Autonomous Region (XZ2020ZR-ZY40(Z) and XZ202101ZR0011G).

Disclosures

None.

Supplemental Material

Expanded Materials & Methods
Figures S1–S6
Major Resources Table
Unedited Gel
References 2,20,43

REFERENCES

1. Fortuno MA, Ravassa S, Fortuno A, Zalba G, Diez J. Cardiomyocyte apoptotic cell death in arterial hypertension: mechanisms and potential management. *Hypertension*. 2001;38:1406–1412. doi: 10.1161/hy1201.099615
2. Wan E, Yeap XY, Dehn S, Terry R, Novak M, Zhang S, Iwata S, Han X, Homma S, Drosatos K, et al. Enhanced efferocytosis of apoptotic cardiomyocytes through myeloid-epithelial-reproductive tyrosine kinase links acute inflammation resolution to cardiac repair after infarction. *Circ Res*. 2013;113:1004–1012. doi: 10.1161/CIRCRESAHA.113.301198
3. Howangyin KY, Zlatanova I, Pinto C, Ngkelo A, Cochain C, Rouanet M, Vilar J, Lemitre M, Stockmann C, Fleischmann BK, et al. Myeloid-epithelial-reproductive receptor tyrosine kinase and milk fat globule epidermal growth factor 8 coordinately improve remodeling after myocardial infarction via local delivery of vascular endothelial growth factor. *Circulation*. 2016;133:826–839. doi: 10.1161/CIRCULATIONAHA.115.020857
4. Zhang S, Weinberg S, DeBerge M, Gainullina A, Schipma M, Kinchen JM, Ben-Sahra I, Gius DR, Yvan-Charvet L, Chandel NS, et al. Efferocytosis fuels requirements of fatty acid oxidation and the electron transport chain to polarize macrophages for tissue repair. *Cell Metab*. 2019;29:443–456.e5. doi: 10.1016/j.cmet.2018.12.004
5. Wang Y, Subramanian M, Yurdagul A Jr, Barbosa-Lorenzi VC, Cai B, de Juan-Sanz J, Ryan TA, Nomura M, Maxfield FR, Tabas I. Mitochondrial fission promotes the continued clearance of apoptotic cells by macrophages. *Cell*. 2017;171:331–345.e22. doi: 10.1016/j.cell.2017.08.041
6. Park D, Han CZ, Elliott MR, Kinchen JM, Trampont PC, Das S, Collins S, Lysiak JJ, Hoehn KL, Ravichandran KS. Continued clearance of apoptotic cells critically depends on the phagocyte UCP2 protein. *Nature*. 2011;477:220–224. doi: 10.1038/nature10340
7. Endeward V, Gros G, Jurgens KD. Significance of myoglobin as an oxygen store and oxygen transporter in the intermittently perfused human heart: a model study. *Cardiovasc Res*. 2010;87:22–29. doi: 10.1093/cvr/cvq036
8. Wilks A. Heme oxygenase: evolution, structure, and mechanism. *Antioxid Redox Signal*. 2002;4:603–614. doi: 10.1089/15230860260220102
9. Lill R, Freibert SA. Mechanisms of mitochondrial iron-sulfur protein biogenesis. *Annu Rev Biochem*. 2020;89:471–499. doi: 10.1146/annurev-biochem-013118-111540
10. Braymer JJ, Freibert SA, Rakwalska-Bange M, Lill R. Mechanistic concepts of iron-sulfur protein biogenesis in biology. *Biochim Biophys Acta Mol Cell Res*. 2021;1868:118863. doi: 10.1016/j.bbamcr.2020.118863
11. Braymer JJ, Lill R. Iron-sulfur cluster biogenesis and trafficking in mitochondria. *J Biol Chem*. 2017;292:12754–12763. doi: 10.1074/jbc.R117.787101
12. Wang T, Cao Y, Zheng Q, Tu J, Zhou W, He J, Zhong J, Chen Y, Wang J, Cai R, et al. Senp1-sirt3 signaling controls mitochondrial protein acetylation and metabolism. *Mol Cell*. 2019;75:823–834.e5. doi: 10.1016/j.molcel.2019.06.008
13. Chiang S, Braidy N, Maleki S, Lal S, Richardson DR, Huang ML. Mechanisms of impaired mitochondrial homeostasis and NAD(+) metabolism in a model of mitochondrial heart disease exhibiting redox active iron accumulation. *Redox Biol*. 2021;46:102038. doi: 10.1016/j.redox.2021.102038
14. Culley MK, Zhao J, Tai YY, Tang Y, Perk D, Negi V, Yu Q, Woodcock CC, Handen A, Speyer G, et al. Frataxin deficiency promotes endothelial senescence in pulmonary hypertension. *J Clin Invest*. 2021;131:e149721.
15. La Rosa P, Petrillo S, Turchi R, Berardinelli F, Schirinzi T, Vasco G, Lettieri-Barbato D, Fiorenza MT, Bertini ES, Aquilano K, et al. The NRF2 induction prevents ferroptosis in Friedreich's ataxia. *Redox Biol*. 2021;38:101791. doi: 10.1016/j.redox.2020.101791
16. Li K, Singh A, Crooks DR, Dai X, Cong Z, Pan L, Ha D, Rouault TA. Expression of human frataxin is regulated by transcription factors SRF and TFAP2. *PLoS One*. 2010;5:e12286. doi: 10.1371/journal.pone.0012286
17. Wagner GR, Pride PM, Babbey CM, Payne RM. Friedreich's ataxia reveals a mechanism for coordinate regulation of oxidative metabolism via feedback inhibition of the SIRT3 deacetylase. *Hum Mol Genet*. 2012;21:2688–2697. doi: 10.1093/hmg/dds095
18. He W, Newman JC, Wang MZ, Ho L, Verdin E. Mitochondrial sirtuins: regulators of protein acylation and metabolism. *Trends Endocrinol Metab*. 2012;23:467–476. doi: 10.1016/j.tem.2012.07.004
19. Wei T, Huang G, Gao J, Huang C, Sun M, Wu J, Bu J, Shen W. Sirtuin 3 deficiency accelerates hypertensive cardiac remodeling by impairing angiogenesis. *J Am Heart Assoc*. 2017;6:e006114. doi: 10.1161/JAHA.117.006114
20. Gao J, Wei T, Huang C, Sun M, Shen W. Sirtuin 3 governs autophagy-dependent glycolysis during angiotensin II-induced endothelial-to-mesenchymal transition. *FASEB J*. 2020;34:16645–16661. doi: 10.1096/fj.202001494R
21. Feng X, Su H, He X, Chen JX, Zeng H. Sirt3 deficiency sensitizes angiotensin-ii-induced renal fibrosis. *Cells*. 2020;9:2510. doi: 10.3390/cells9112510
22. Zhang Y, Wang Y, Zhou D, Zhang LS, Deng FX, Shu S, Wang LJ, Wu Y, Guo N, Zhou J, et al. Angiotensin II deteriorates advanced atherosclerosis by promoting mertk cleavage and impairing efferocytosis through the at1r/ros/p38 mapk/adam17 pathway. *Am J Physiol Cell Physiol*. 2019;317:C776–C787. doi: 10.1152/ajpcell.00145.2019
23. Scott RS, McMahon EJ, Pop SM, Reap EA, Caricchio R, Cohen PL, Earp HS, Matsushima GK. Phagocytosis and clearance of apoptotic cells is mediated by mer. *Nature*. 2001;411:207–211. doi: 10.1038/35075603
24. Cai B, Thorp EB, Doran AC, Sansbury BE, Daemen MJ, Dorweiler B, Spite M, Fredman G, Tabas I. Mertk receptor cleavage promotes plaque necrosis and

defective resolution in atherosclerosis. *J Clin Invest*. 2017;127:564–568. doi: 10.1172/JCI90520
25. Carrillo I, Rabelo RAN, Barbosa C, Rates M, Fuentes-Retamal S, Gonzalez-Herrera F, Guzman-Rivera D, Quintero H, Kemmerling U, Castillo C, et al. Aspirin-triggered resolvin d1 reduces parasitic cardiac load by decreasing inflammation in a murine model of early chronic Chagas disease. *PLoS Negl Trop Dis*. 2021;15:e0009978. doi: 10.1371/journal.pntd.0009978
26. Suresh Babu S, Thandavarayan RA, Joladarashi D, Jeyabal P, Krishnamurthy S, Bhimaraj A, Youker KA, Krishnamurthy P. Microrna-126 overexpression rescues diabetes-induced impairment in efferocytosis of apoptotic cardiomyocytes. *Sci Rep*. 2016;6:36207. doi: 10.1038/srep36207
27. Gerlach BD, Ampomah PB, Yurdagul A Jr, Liu C, Lauring MC, Wang X, Kasikara C, Kong N, Shi J, Tao W, et al. Efferocytosis induces macrophage proliferation to help resolve tissue injury. *Cell Metab*. 2021;33:2445–2463.e8. doi: 10.1016/j.cmet.2021.10.015
28. Ampomah PB, Cai B, Sukka SR, Gerlach BD, Yurdagul A Jr, Wang X, Kuriakose G, Darville LNF, Sun Y, Sidoli S, et al. Macrophages use apoptotic cell-derived methionine and dnmt3a during efferocytosis to promote tissue resolution. *Nat Metab*. 2022;4:444–457. doi: 10.1038/s42255-022-00551-7
29. Shi H, Duan J, Wang J, Li H, Wu Z, Wang S, Wu X, Lu M. 1,25(oh)(2)d(3) promotes macrophage efferocytosis partly by upregulating asap2 transcription via the vdr-bound enhancer region and asap2 may affect antiviral immunity. *Nutrients*. 2022;14:4935. doi: 10.3390/nu14224935
30. Viaud M, Ivanov S, Vujic N, Duta-Mare M, Aira LE, Barouillet T, Garcia E, Orange F, Dugail I, Hainault I, et al. Lysosomal cholesterol hydrolysis couples efferocytosis to anti-inflammatory oxysterol production. *Circ Res*. 2018;122:1369–1384. doi: 10.1161/CIRCRESAHA.117.312333
31. Yurdagul A Jr, Subramanian M, Wang X, Crown SB, Ilkayeva OR, Darville L, Kolluru GK, Rymond CC, Gerlach BD, Zheng Z, et al. Macrophage metabolism of apoptotic cell-derived arginine promotes continual efferocytosis and resolution of injury. *Cell Metab*. 2020;31:518–533.e10. doi: 10.1016/j.cmet.2020.01.001
32. Cai S, Zhao M, Zhou B, Yoshii A, Bugg D, Villet O, Sahu A, Olson GS, Davis J, Tian R. Mitochondrial dysfunction in macrophages promotes inflammation and suppresses repair after myocardial infarction. *J Clin Invest*. 2023;133:e159498. doi: 10.1172/JCI159498
33. Song CX, Chen JY, Li N, Guo Y. Ctrp9 enhances efferocytosis in macrophages via mapk/drp1-mediated mitochondrial fission and adipor1-induced immunometabolism. *J Inflamm Res*. 2021;14:1007–1017. doi: 10.2147/JIR.S302944
34. Soares MP, Hamza I. Macrophages and iron metabolism. *Immunity*. 2016;44:492–504. doi: 10.1016/j.immuni.2016.02.016
35. Read AD, Bentley RE, Archer SL, Dunham-Snary KJ. Mitochondrial iron-sulfur clusters: structure, function, and an emerging role in vascular biology. *Redox Biol*. 2021;47:102164. doi: 10.1016/j.redox.2021.102164
36. Richardson DR, Lane DJ, Becker EM, Huang ML, Whitnall M, Suryo Rahmanto Y, Sheftel AD, Ponka P. Mitochondrial iron trafficking and the integration of iron metabolism between the mitochondrion and cytosol. *Proc Natl Acad Sci USA*. 2010;107:10775–10782. doi: 10.1073/pnas.0912925107
37. Pandolfo M. Frataxin deficiency and mitochondrial dysfunction. *Mitochondrion*. 2002;2:87–93. doi: 10.1016/s1567-7249(02)00039-9
38. Silva AM, Brown JM, Buckle VJ, Wade-Martins R, Lufino MM. Expanded GAA repeats impair FXN gene expression and reposition the FXN locus to the nuclear lamina in single cells. *Hum Mol Genet*. 2015;24:3457–3471. doi: 10.1093/hmg/ddv096
39. Punga T, Buhler M. Long intronic GAA repeats causing friedreich ataxia impede transcription elongation. *EMBO Mol Med*. 2010;2:120–129. doi: 10.1002/emmm.201000064
40. Roszer T. Adipose tissue immunometabolism and apoptotic cell clearance. *Cells*. 2021;10:2288. doi: 10.3390/cells10092288
41. Madenspacher JH, Morrell ED, Gowdy KM, McDonald JG, Thompson BM, Muse G, Martinez J, Thomas S, Mikacenic C, Nick JA, et al. Cholesterol 25-hydroxylase promotes efferocytosis and resolution of lung inflammation. *JCI Insight*. 2020;5:e137189. doi: 10.1172/jci.insight.137189
42. Liao J, Xie Y, Lin Q, Yang X, An X, Xia Y, Du J, Wang F, Li HH. Immunoproteasome subunit beta5i regulates diet-induced atherosclerosis through altering mertk-mediated efferocytosis in apoe knockout mice. *J Pathol*. 2020;250:275–287. doi: 10.1002/path.5368
43. Maidana DE, Tsoka P, Tian B, Dib B, Matsumoto H, Kataoka K, Lin H, Miller JW, Vavvas DG. A novel imagej macro for automated cell death quantitation in the retina. *Invest Ophthalmol Vis Sci*. 2015;56:6701–6708. doi: 10.1167/iovs.15-17599